Macroion Clustering in Solutions and Suspensions: The Roles of Microions and Solvent

ARTICLE *in* THE JOURNAL OF PHYSICAL CHEMISTRY B · APRIL 2009

Impact Factor: 3.3 · DOI: 10.1021/jp805648a · Source: PubMed

1 AUTHOR:

Kenneth Schmitz
University of Missouri - Kansas City
85 PUBLICATIONS **1,420** CITATIONS

SEE PROFILE

THE JOURNAL OF PHYSICAL CHEMISTRY B

Article

Macroion Clustering in Solutions and Suspensions: The Roles of Microions and Solvent

Kenneth S. Schmitz

J. Phys. Chem. B, **2009**, 113 (9), 2624-2638• DOI: 10.1021/jp805648a • Publication Date (Web): 05 January 2009

Macroion Clustering in Solutions and Suspensions: The Roles of Microions and Solvent†

Kenneth S. Schmitz

Department of Chemistry, University of Missouri - Kansas City, Kansas City, Missouri, 64110

Received: June 20, 2008; Revised Manuscript Received: November 5, 2008

Under certain conditions, macroion systems undergo a transition from a homogeneous state to a heterogeneous state in regard to spatial configurations and dynamic processes. Examined herein are three specific cases: highly ordered "crystalline-like" structures with very little kinetic activity in equilibrium with disordered spatial regions that exhibit normal diffusive motions, as first examined by Ise and co-workers (class I); an anomalously slow relaxation domain coexisting with "normal" relaxation modes but with no spatially ordered regions, as first reported by Schurr and co-workers (class II); and the formation of "vesicle-like" structures by inorganic molybdenum oxide macroions (polyoxometalates, POM), as examined in detail by Liu and co-workers (class III). A common feature of these three cases is that the heterogeneous structures do not involve macroions in physical contact, thereby ruling out the possibility of van der Waals attraction as the source of attraction. The commonalities of these three cases are that they involve electrostatic attraction as mediated by counterion and polar solvent structures, the extent of which is a function of the charge magnitude, distribution of charge on the macroion surface, and the relative macroion−solvent particle sizes. The results of juxtaposition of potential fields (JPF) profiles and Brownian dynamics (BD) simulations on these three systems suggest a family of states in the *charge-size* landscape of heterogeneous configurations.

1. Introduction

The DLVO theory (Derjguin−Landau−Verwey−Overbeek)[1] for the pair potential between charged colloids is a popular model for interpreting data on colloidal systems. The form of the DLVO potential is a repulsive screened Coulomb term plus an *ad hoc* addition of a short-range attraction van der Waals term. It thus served its purpose in the explanation of the stability of colloidal particles (long-range electrostatic repulsion) and the "sticking together" of colloidal particles separated, at most, by a few angstroms (short-range van der Waals attraction). In the last quarter of the 20th century, data appeared in the literature that could not be explained by the DLVO theory. In particular, the systems exhibited heterogeneous structure in both space and time, where the particles were separated by several hundreds of angstroms.

Ise and co-workers, using video imagery methods,[2,3] reported trajectories on highly charged polymer latex suspensions that showed extensive kinetic activity in the spatially "random" region along with crystalline-like regions of virtually no kinetic activity. Also, studies on highly charged silica latex particles clearly indicated large void regions in apparent equilibrium with dense regions.[4−6] Such a situation of voids and kinetically different regions would be unstable for a system of macroions interacting only through a highly repulsive potential. Furthermore, the average spacing between the macroions in the crystalline-like region was reported to be smaller than that based on concentration, which means some form of attraction exists between these macroions. Since the electrostatic interaction between macroions is repulsive, the source of this long-range attraction must somehow involve the disposition of the microions. Highly charged macroion and colloidal systems with these characteristics are referred to as class I systems.

Macroions of intermediate charge also exhibit unusual dynamic behavior. Schurr and co-workers[7−9] used dynamic light scattering (DLS) methods to follow the dynamics of poly-L-lysine [molecular weight $M = 200\,000$, which corresponds to a degree of polymerization of $n = 955$ and denoted as $(\mathrm{lys})_n = (\mathrm{lys})_{955}$] as a function of added salt. As the added electrolyte concentration was decreased to about 5 mM, the apparent diffusion coefficient, D_{app}, increased in value as one would expect with an increased repulsive interaction between the polyions. However, further lowering of the added salt gave an unexpected result: over a very narrow ionic strength range, D_{app} exhibited a *dramatic drop in value*, by a factor of 20, accompanied by a decrease by only a factor of 2 in light scattering intensity. Since in their study only one relaxation mode was detected on either side of the transition point, they referred to this transition as the "ordinary−extraordinary phase transition" (o−e transition). DLS studies by Drifford and Dalbiez[10,11] also indicated an o−e transition for poly(styrene sulfonate). These authors obtained an empirical expression that related the location of the o−e transition to the concentrations of the macroions and the microions and their respective charges

$$\frac{C_m\langle b\rangle}{Z_s\lambda_B\left(\sum C_jZ_j^2\right)} = \frac{n_m4\pi\langle b\rangle}{Z_s}\frac{1}{4\pi\lambda_B\left(\sum n_jZ_j^2\right)} = \frac{n_m4\pi\langle b\rangle\lambda_{DH}^2}{Z_s} = 1 \quad (1.1)$$

where $\lambda_B = (q_e)^2/\varepsilon k_BT$ is the Bjerrum length, q_e is the electron charge, ε is the bulk dielectric constant, k_B is the Boltzmann constant, T is the absolute temperature, C_j (n_j) is the molar (number) concentration of the jth ion of valency Z_j, C_m (n_m) is the molar (number) concentration of monomer units, $\langle b\rangle$ is the average spacing between charges on the linear polyion, Z_s is

† Part of the "J. Michael Schurr Special Section".

10.1021/jp805648a CCC: $40.75
Published on Web 01/05/2009

the valency of the counterion of added salt, and $\lambda_{DH} = 1/\kappa_{DH}$ is the Debye−Hückel screening length for the *added* electrolyte. It was shown that eq 1.1 can be expressed in terms of the ratio of "effective volumes" for the unit charge of the counterion along the cylindrical axis (V_s) and the monomer ($V_m = 1/n_m$).[12]

$$1 = 4\frac{[(\pi\lambda_{DH}^2\langle b\rangle)/Z_s]}{n_m^{-1}} = 4\left(\frac{V_s}{V_m}\right) \qquad (1.2)$$

The interpretation of eq 1.2 is that the onset of the o−e transition is when the ion clouds of the macroions begin to overlap. This observation led to a "temporal aggregate" model in which the slow mode represented the decay of a macroion cluster held together by the sharing of counterions.[13,14] Charged systems with these characteristics are referred to as class II systems.

Another class of molecules that form superstructures believed to be stabilized by counterion-mediated attraction is exemplified by "vesicle-like" structures of giant polyoxometalate (POM) macroions. The POM macroions are mainly hydrophilic giant metal-oxide molecular clusters which have a well-defined molecular structure, mass, and shape. The metal centers are generally transition metals such as molybdenum, tungsten, and vanadium (with variable oxidation states, such as V and VI in the case of Mo). Only the number of central metal ions is given in the simplified notation, such as $\{Mo_X\}$ for polyoxomolybdates. These nanoscaled inorganic molecules possess beautiful and sometimes symmetric shapes: hollow spheres $\{Mo_{132}\}$[16] and $\{Mo_{72}Fe_{30}\}$;[16,18,19] wheel-shaped $\{Mo_{154}\}$[17] and $\{Mo_{176}\}$; and "hedgehog"-shaped $\{Mo_{368}\}$.[15] Coordinated to their external surfaces of these large POMS are a large number of water ligands that make them very hydrophilic, and thus render these clusters very soluble in polar solvents. Most POM clusters are charged macroanions, where the common cations may be Na^+, K^+, NH_4^+, and H^+. Partial deprotonation of the water ligands may also contribute to the charge of the macroion, such as in the case of $\{Mo_{72}Fe_{30}\}$. Of specific interest herein is the interesting property of some POM macroions to self-assemble into larger structures, even in dilute solutions, to form "vesicle-like" superstructures, as deduced from the equivalence of the hydrodynamic radius (R_h) and the radius of gyration (R_g) determined from DLS and static light scattering (SLS) methods, respectively. Since no superstructures are formed when the POMs are neutrally charged in solution, van der Waals attraction is not responsible for the formation of the hollow sphere structures. Liu and co-workers suggested that the stability of the vesicle structure was due to a balance between counterion-mediated electrostatic effects, van der Waals forces, and hydrogen bonding where the counterions are positioned between the macroions.[18,20] Low charged macroions that form well-defined assemblies that are stabilized by polar solvent and counterion-mediated interactions define the class III heterogeneous system.

A common feature of these defined classes of macroions is the necessary involvement of microions in the regulation of the effective charge and the attractive interaction between the macroions in the heterogeneous state of the system. The Langmuir model for coacervates[21] provides a viable platform for the interpretation of the heterogeneous structures over the range of high to low macroion charges. To explain the equivalence of the chemical potential of the micelles in both states in the heterogeneous regime, Langmuir proposed that the effective charge of each micelle in the cluster was less than those in the "free" state. To explain the stability of the cluster, Langmuir proposed that the macroions and counterions are arranged in an array similar to that of a sodium chloride crystal of alternating positive and negative charges. Summation of all possible pairs in the crystal array results in a net negative energy, which is indicative of a stable configuration. This model thus takes into account the interactions of one macroion with the counterions surrounding all other macroions, which Langmuir[21] pointed out was one shortcoming of the DLVO model.

However, unlike the atoms in the salt crystal, the macroions and microions are in constant motion. Hence, the static "Langmuir crystal" of alternating macroions and counterions must be modified to paint a dynamic picture. We adopt, therefore, the quantum mechanical view of atoms and electrons in the formation of molecules in an "orbital" description of the microions in a macroion environment. Just as some of the electrons are held close to the parent nucleus while others participate in either localized or delocalized chemical bonds, some of the counterions are tightly held about one macroion to give rise to the "effective charge" while other counterions are shared between macroions in the form of "orbitals" embracing the collection of macroions. It is thus the "delocalized sharing" of these counterions that gives rise to a correlation in the dynamics of the macroions comprising the "cluster". This view is extended to include stabilization of "vesicle-like" structures formed by inorganic molybdenum macroions that are comparable in size to the solvent molecules, which are stabilized by the polar solvent through the formation of "solvent bridges" and counterions. Thus, heterogeneous systems may be viewed as a continuum family of systems on a *charge-size* landscape of heterogeneous configurations.

The present paper explores in more detail the collective electric fields set up by a cluster of macroions and the corresponding effects on the dispositions of the microions and/or solvent structures. The juxtaposition of potential fields (JPF) method[22] provides a basis for identifying "orbitals" as bounded by constant potential surfaces in a manner similar to that of Bader and co-workers[23,24] to identify bonds between atoms in molecules. How these potential profiles affect the macroion systems is dependent upon the magnitude and distribution of the charge on the macroion, and the relative size of the macroion to that of the solvent.

2. The Charge-Size Heterogeneous Landscape

The *charge-size* heterogeneous landscape is defined as that subset of solution/suspension states of a system in which macroions of like charge exist in clusters that are stabilized by electrostatic interactions rather than van der Waals interactions. Because the macroions are of like charge, the stabilizing mechanism must involve counterions for all systems considered herein. When viewed from afar, the macroion may be treated as a "point charge", since any dependence of the potential field on the structural integrity and charge distribution becomes inconsequential. However, such structural details are very important in the vicinity of the macroion. In the case of macroions of size comparable to a polar solvent, there is the additional, and perhaps necessary, involvement of the solvent in the stabilization mechanism. In this case, the site charges and their distributions play an important role in the organization of the solvent particles.

The classification of electrostatic interactions as "strong", "intermediate", and "weak" is determined, in this discussion, by the interaction of a "test probe" with the site charges of the macroion. By using a test probe, the *net charge* on the macroion is the appropriate descriptive parameter of the macroion charge

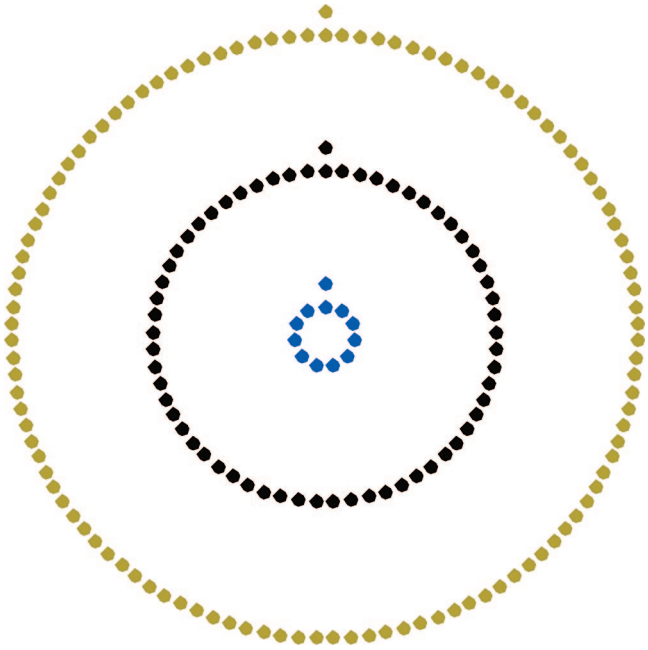

Figure 1. Interaction of a test charge with constant charge density circles. The total charges on the three circles that represent the three charge classes are $Z_I = 111$ (high), $Z_{II} = 61$ (intermediate), and $Z_{III} = 11$ (weak). The radius of the smallest circle is set at $R_{small} = 1$ with the other two appropriately chosen to maintain a constant linear charge density, and the test charge is placed a relative distance of 0.8 from the site charge at the apex of each circle. The total interaction energies U_n of the test charge with the site charges, represented as reciprocal distances in eq 2.1, for the three circles are $U_{111} = 15.676$, $U_{61} = 13.353$, and $U_{11} = 6.691$.

rather than the surface charge density in the determination of which "electrostatic strength class" a macroion belongs. This is because macroions may have the same surface charge density but exhibit different strengths of interaction with the test probe.

To illustrate the ambiguity in classification that might arise by using surface charge density as an electrostatic classification parameter, we consider three circles with the same linear charge density but different total charges. For the purpose of illustration, the total charges for the three classifications, indicated by the subscripts, are taken to be $Z_I = 111$, $Z_{II} = 61$, and $Z_{III} = 11$. The circumference is chosen to maintain a constant linear charge density with the smallest circle of radius $R_{small} = 1$. A "test probe" counterion is placed a relative distance of 0.8 from the center of the site at the apex of the circle. The three circles are shown in Figure 1. The relative interaction energy of the system with n sites, U_n, is represented by the summation of reciprocal distances between the test probe and each discrete site charge on the ring, i.e.,

$$U_n = \sum_{i=1}^{n} \frac{1}{r_{ic}} \tag{2.1}$$

where r_{ic} is the distance between the centers of site i and the test probe c. The results for these three rings are $U_{11} = 6.691$, $U_{61} = 13.353$, and $U_{111} = 15.676$. Hence, if one were to construct a binding isotherm using the total interaction between all of the discrete sites on the circle, one would conclude that the test probe conterion is "more tightly bound" by the circle with the higher charge even though the linear charge densities are the same for all three systems.

This exercise with circles indicates that three macroions may have exactly the same surface charge density but could fall into three different charge classifications in the *charge-size* heterogeneous landscape. A corollary is that *surface charge density is not a viable parameter to classify the electrostatic strengths of macroions*. In other words, three macroions with the same surface charge density may reside in the *strong*, *intermediate*, and *weak* charged systems.

3. Juxtaposition of Potential Fields/Orbital Model for Macroion Systems

The JPF method follows the quantum mechanical prescription of finding the energy of a molecule. Because the microions move more rapidly than the macroions, the macroions may be considered to be fixed in space while the microions seek their equilibrium distributions. The potential field set up by the macroions corresponds to the electric potential set up by the nuclei in the molecule. The reduced potential field set up at any arbitrary point in the solvent system by a collection of M identical macroions of radius a_p and charge Z_p is defined as

$$\phi_{mac}(r) = Z_p\left(\frac{\lambda_B}{a_p}\right)\sum_{J=1}^{M}\frac{1}{|\mathbf{r}_J|} = \sum_{J=1}^{M}\phi_J(\mathbf{r}) \tag{3.1}$$

The reduced scalar distance $|\mathbf{r}_J|$ has the components $\mathbf{r}_J = \{(x - x_J)/a_p, (y - y_J)/a_p, (z - z_J)/a_p\}$, as measured from the center of the Jth macroion to the point of interest in the medium and expressed in units of the macroion radius a_p. From the Gibbs−Duhem expression, we have the following relationship between the reduced macroion potential and the chemical potential of the microions at position $\mathbf{r}$ for fixed macroion locations

$$\nabla\phi_{mac}(\mathbf{r}) + \beta\nabla\mu_{ideal}(\mathbf{r}) + \beta\nabla\mu_{nonideal}(\mathbf{r}) = 0 \tag{3.2}$$

where ∇ is the spatial gradient operator, $\beta = 1/k_BT$, and the ideal and nonideal components of the chemical potentials of the microions are separately expressed. If one were to ignore the nonideal contributions to the chemical potential, then the landscape provided by the macroion field $\phi_{mac}(\mathbf{r})$ mimics the distribution of the counterions and added ions of like sign, collectively referred to as counterions. Counterions in those orbitals tightly wrapped about a single macroion may serve to alter the "effective charge" of that macroion. Those orbitals which encompass several macroions are analogous to "bonding orbitals" in the molecules.

The validity of these interpretations of the JPF profiles and orbital pictures is found in the computer simulations of Sánchez-Sánchez and Lozada-Cassou[25] for two approaching macroions, and the Brownian dynamics (BD) for clusters of 7 macroions[26,27] and 16 macroions[27] in the presence of added electrolyte.

Sánchez-Sánchez and Lozada-Cassou[25] used a three-point extension to the hypernetted chain/mean spherical integration equation (HNC/MSI) to study the distribution of counterions in the vicinity of two macroions. The parameters in their study were the following: macroions of radius $a_p = 7$ Å; counterions of diameter $d_c = 4.25$ Å; an added 1:1 salt concentration of 0.01 M; and a macroion surface charge density of $\sigma = 0.1$ C/m^2. The surface-to-surface separation distances, τ, between the macroions that are of interest are $\tau = 5d_c$ and $\tau = 2d_c$. The equivalent system in the JPF simulations are macroions of radius $a_p = 7$ Å and a charge of $Z_p = 4$. The center-to-center separation

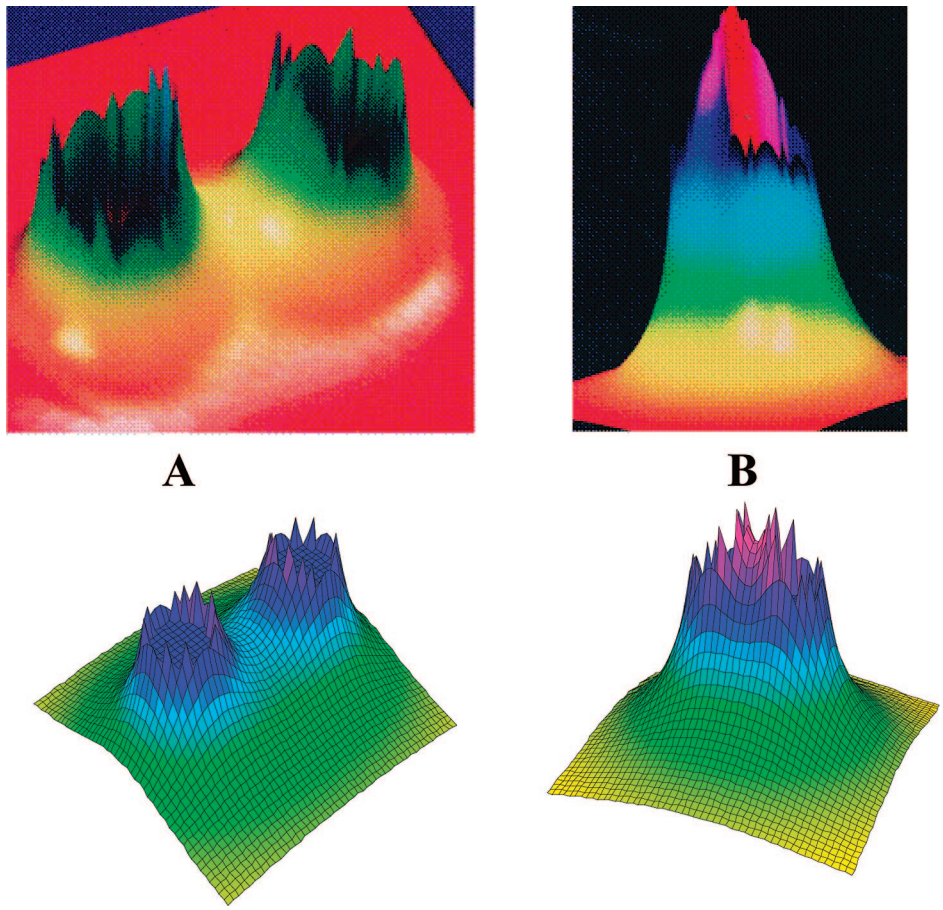

Figure 2. Comparison of the HNC/MSI and JPF methods. The top figures are results for the three-point extension to the hypernetted chain/mean spherical integration equation (HNC/MSI) reported by Sánchez-Sánchez and Lozada-Cassou[25] for two macroions of radius $a_p = 7$ Å and surface charge density $\sigma = 0.1$ C/m^2; the diameter of the counterion was $d_c = 4.25$ Å, and the added salt concentration was 0.01 M. The surface-to-surface distances of closest approach were $\tau = 5d_c$ (top A) and $\tau = 2d_c$ (top B). These pictures were kindly provided by Marcelo Lozada-Cassou for adaptation. The bottom figure is a JPF contour plot of ϕ_{mac} in the reduced X_r-Y_r plane for an equivalent system of macroions with radius $a_p = 7$ Å and net charge $Z_p = 4$. The equivalent center-to-center distances $\tau + 2a_p$, normalized to the radius of the macroion, a_p, are $D_{sep} = (\tau + 2a_p)/a_p = 5$ (bottom A) and $D_{sep} = 3.2$ (bottom B).

distances are normalized to the particle radius, $D_{sep} = (\tau + 2a_p)/a_p$. The value of ϕ_{mac} at the surface and in the interior of each macroion was taken to be the surface potential of the isolated macroion, $\phi_J(|\mathbf{r}| = a_p)$. Shown in Figure 2 are comparisons of the HNC/MSI results (Figure 2, top) with the JPF potential ϕ_{mac} in the X_r-Y_r plane (Figure 2, bottom). The similarities in the A and B profiles for the two methods indicate that the quantitative results of the HNC/MSI method are faithfully reflected in the qualitative profiles of the JPF method. In both cases for $D_{sep} = 5$ (Figure 2A, top and bottom), the two macroions are easily discernible. As indicated in Figure 2A, bottom, ϕ_{mac} in the vicinity of the macroion surface is slightly larger than the surface potential for the isolated macroion. This means that the counterions accumulate in the vicinity of each macroion, and the counterion concentrations decrease in all directions as one moves away from each macroion. However, as the two macroions are brought in close proximity such that $D_{sep} = 3.2$, the two macroions are completely engulfed by the counterion distribution, as indicated in the HNC/MSI results in Figure 2B, top. This means that the concentration of the counterions between the macroions is greatly enhanced relative to that in Figure 2A, top. Similarly, the JPF method shows that ϕ_{mac} obscures the identity of either macroion, as shown in Figure 2B, bottom.

BD simulations were carried out for the movement of microions in the presence of a fixed array of macroions.[26,27] The total force F_j acting on the jth microion was of the form

$$F_j = -Z_j\nabla_j\left(\varphi_{mac}(\mathbf{r}_j) + \left(\frac{\lambda_B}{a_p}\right)\sum_{i\neq j}\frac{Z_i}{|\mathbf{r}_{ji}|}\right) \qquad (3.3)$$

where $\phi_{mac}(\mathbf{r}_j)$ is the reduced macroion potential defined by eq 3.1 at the location of the jth microion and the second term in parentheses is the reduced potential for the ith microion on the jth microion at a separation distance $|\mathbf{r}_{ji}|$. The simulations were carried out in two steps: a "pre-equilibrium calculation" of 10^6 cycles for *each* of the microion coordinates, followed by a "thermodynamic calculation" of *at least* 10^6 iterations for each of the coordinates of all of the microions. The movement of all microions constitutes one iteration cycle. To display the results of the thermodynamic calculation, the volume of the system was divided into equal sized cubic bins. At the conclusion of each iteration cycle, the occupancy of microions in each bin was determined separately for the counterions and the co-ions, and added to the sum of the previous iteration cycles. The microion density function $S(X_r, Y_r, Z_r)$ was defined as the number of particles in the bin whose center is located at $\{X_r, Y_r, Z_r\}$ at the end of the simulation divided by the number of iterations. Because the concentration of counterions was so high in the vicinity of the macroion, a relative distribution function for the

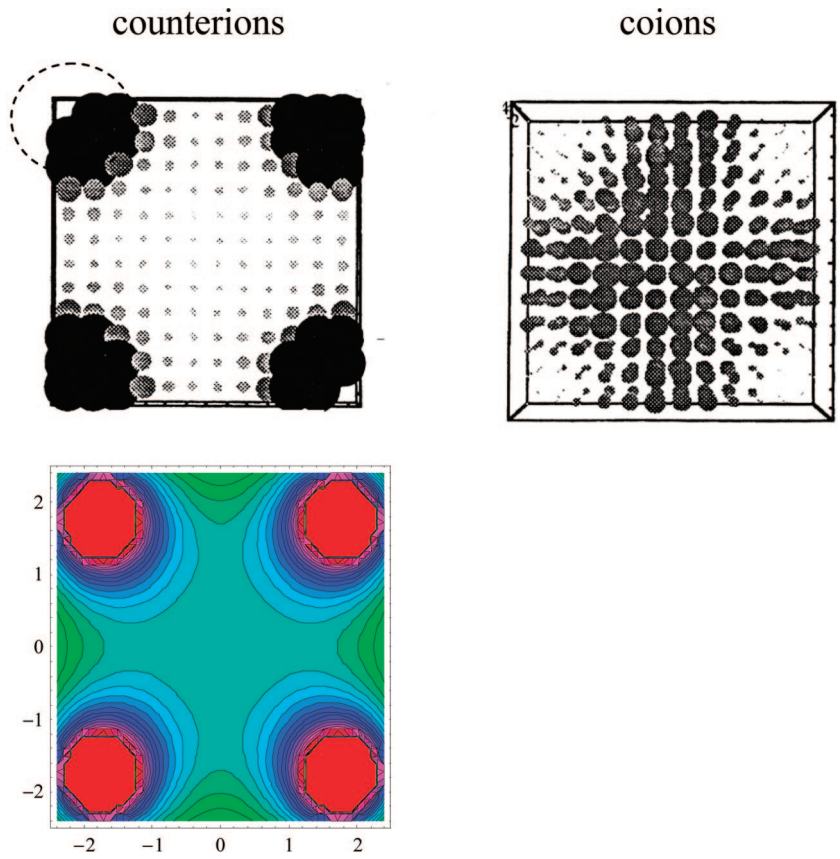

Figure 3. Brownian dynamics and JPF simulations of microion distributions in a cubic array of macroions. BD simulations of the counterion and co-ion distributions were performed for a 2 × 2 × 4 fixed cubic array with lattice constant CC = 3.5 of macroions of charge $Z_p = 50$ and $a_p = 100$ Å. Shown above is a region selected at the interior of the array over the range $4.5 \geq Z_r \geq 2.5$, where the dashed circle represents the location of one macroion in the lattice. The relative distributions of counterions and co-ions are reflected in the size of the dots within each subcell, as described in the text. Shown at the bottom are the JPF constant contours of ϕ_{mac} for the interior of a 4 × 4 × 4 cubic array of the macroions.

counterions was defined by dividing members of the set $\{S_k\}$ by the largest member, S_{max}, viz., $s_k = S_k/S_{max}$. One can now represent the relative distribution of microions by the radius and shading of a sphere located in each subcell. For example, for the case $s_k = 1$, the radius of the sphere is equal to half the length of a side of the subcell, $R_k = L_{subcell}/2$, and the color of the sphere is black. Other density values would be represented by spheres of smaller radii and varying shades of gray.

The system is a 2 × 2 × 4 array of macroions of charge $Z_p = 50$ and radius $a_p = 100$ Å with a lattice spacing of CC = 3.5 at a volume fraction $\varphi_p = 0.01$, with 50 added 1:1 salt particles of radius $a_c = 1$ Å for a total of 900 microions. The counterion and co-ion distributions in the slice $4.5 \geq Z_r \geq 2.5$ are shown in Figure 3, top. As expected, the counterions congregated in the vicinity of the macroions at concentrations much higher than in the interior of the cluster, and the co-ions congregate more to the center of the interior of the cluster. The constant potential profile at $Z_r = 0$ in the $X_r - Y_r$ plane, shown in Figure 3, bottom, likewise reflects the accumulation of counterions in the vicinity of each macroion. Shown in Figure 4 are the constant potential surfaces for the values $\phi_{mac} = 38$ (red), $\phi_{mac} = 36$ (blue), and $\phi_{mac} = 34$ (green). These constant potential surfaces represent the orbital model of the cluster. The analogy with a molecular orbital arises from the fact that counterions that interact only with the macroion field may freely move by random motion on these surfaces, since there is no force parallel to the surface. The "red orbitals" are localized about individual macroions and hence are not "bonding orbitals". However, counterions in this orbital may function to reduce the effective charge of the macroion. Counterions located in the "blue orbital" can freely move among the eight macroions of the interior unit cell. This "sharing" of counterions through "delocalized orbitals" is analogous to the overlap of ion clouds between neighboring macroions. Finally, the "green orbital" envelops all of the macroions in the system as expected for counterions in the "free" solution.

4. Class I - Highly Charged Macroions in an Ordered Array

We begin our trek along the landscape of spatial and dynamic heterogeneity in charged systems with the highly charged macroions. If the interaction between the macroions was purely repulsive, then intuitively one might expect a long-range crystalline structure throughout the volume, resulting from a minimization of energy principle in accordance with the DLVO potential. However, this intuition is not supported by the experimental evidence.

To examine the effect of smaller lattice parameters on the disposition of the microions, BD simulations were performed on the system described in Figure 3 but at a lattice distance CC = 2.5. The results, shown in Figure 5, top, indicate a much larger accumulation of counterions in the vicinity of the macroions with virtually an *exclusion* of co-ions in the interior of the cluster. The influx of counterions is reflected in the corresponding JPF constant potential profile shown in Figure 5, bottom. In comparison with Figure 3, bottom, there is a greater distortion of the orbitals about the macroions toward the center of the cluster, as would be expected by the superposition of the potential fields. The orbital structure for

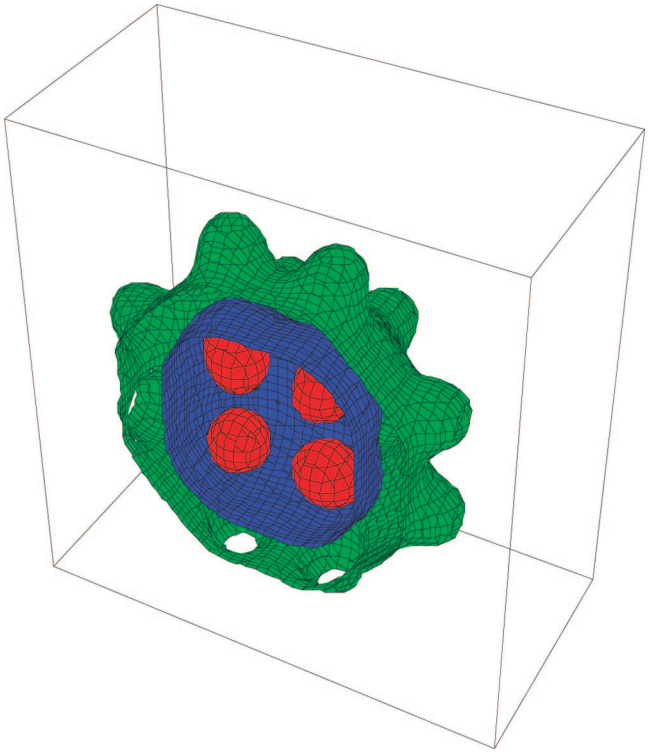

Figure 4. Orbitals of the cubic array of macroions. For illustration purposes to show the JPF orbitals, only the positive X_r coordinates of the cubic array described in Figure 3 are shown above. The constant potential values are $\phi_{mac} = 38$ (red), $\phi_{mac} = 36$ (blue), and $\phi_{mac} = 34$ (green). Since there is no force acting on the counterions within each surface, the constant potential surfaces represent "orbitals" by analogy with chemical bonding.

CC = 2.5 is shown in Figure 6 for $\phi_{mac} = 34$, 36, 38, and 54. In comparison with the orbitals in Figure 4 for CC = 3.5, the orbitals corresponding to $\phi_{mac} = 38$ and $\phi_{mac} = 36$ now encompass the entire cluster rather than the individual macroions and unit cell macroions, respectively. Localized orbitals about individual macroions are now obtained for $\phi_{mac} = 54$, which means that more counterions are in the vicinity of a macroion at the smaller lattice spacing than for the larger lattice spacing.

The orbital model provides the following interpretation of the heterogeneous state in which void regions are observed. As the macroions in a cluster are drawn closer together, more counterions are drawn to the interior of the cluster. Because of the increase in the cumulative macroion potential ϕ_{mac} in the vicinity of any one macroion, the local concentration of the "bound" counterions will reduce the "effective charge" of a macroion in the cluster relative to that of the macroion in the less dense region. A similar explanation was given by Langmuir to establish an equivalent chemical potential between the dense and less dense regions of micelles.[21] Furthermore, the local charge density of the counterions might exceed the local charge density of the macroions. With such a large local concentration of counterions, the law of mass action may lead to "overcharging" of a macroion, i.e., a charge reversal. Overcharging has been viewed as a possible mechanism of attraction between macroions of like charge.[28−32] Mukherjee and co-workers[33,34] used energy minimization (EM) methods to study the distribution of counterions on macroions of various geometries and charge distributions. The reference state was the macroion with N_c neutralizing counterions distributed on its surface in accordance with the EM method. Upon addition of n "overcharging" counterions, a new distribution of surface-bound conterions was determined. The results were presented as the reduced energy differences between the reference state and that for a system of n "overcharging counterions", i.e., $\Delta E_n/k_BT$ versus n. In all cases examined, monovalent as well as divalent counterions, a plot of $\Delta E_n/k_BT$ versus n exhibited an initial decrease (more negative), passed through a minimum, and then increased (less negative). In other words, stable overcharged structures are obtained for all simulations as long as the number of excess counterions is small such that the total macroion−counterion attraction energy exceeded the total counterion−counterion repulsion energy. The overcharging need not be a global effect that changes the sign of the net charge of the macroion. Overcharging of local regions on the macroion surface would likewise give rise to an electrostatic attraction when the overcharged surface is aligned with the charged surface of a neighboring macroion. A similar mechanism was proposed involving "anti-correlation" interactions between screening counterions on planar surfaces.[35]

5. Class II - Intermediate Charged Macroions and Dynamic Heterogeneity

The class II macroions are defined by the o−e transition exhibited by certain macroions such as poly(lysine). What is unusual about the o−e transition for $(lys)_n$ is that *no other measurement gives such dramatic changes as in the DLS experiments*. For example, Zero and Ware[36] used FRAP (fluorescence recovery after photobleaching) methods to obtain values of the self, or tracer, diffusion coefficient (D_T) for $(lys)_{430}$ ($M = 90\,000$) through the transition region. They reported that D_T exhibited a smooth and continuous decrease in value by a factor of about 2 over the salt concentration range examined, *which included the o−e transition region*. As noted by Ware, the FRAP experiment is sensitive enough to detect any aggregates that may be formed. The following are characteristic at the o−e transition point: the relative viscosity exhibited a small maximum;[37] the equivalent conductance indicated a slight vertical displacement;[38] and the electrophoretic mobility obtained by electrophoretic light scattering (ELS) indicated a small change in slope.[36,39] That the $(lys)_n$ are not in physical contact is also supported by the fluorescence labeling studies of Bruno and Mattice[40,41] for $(lys)_n$ over the molecular weight range 15 000−30 000. They reported that the Förster energy transfer occurred between the $(lys)_n$ molecules separated by distances comparable to the average separation distance based on the concentration.

DLS studies by Ramsay and Schmitz[14,42] on higher molecular weight $(lys)_{3800}$ ($M = 800\,000$) indicated that the "extraordinary phase" was not composed of a single relaxation process. Rather, the "extraordinary phase" was characterized by a "splitting" into two widely separated relaxation domains: a "fast" relaxation process which is a *continuation of the relaxation process* characteristic of the "ordinary phase" and an anomalously "slow" relaxation process. The "extraordinary phase" is not, therefore, a "true homogenous phase" but rather a heterogeneous state composed of normal diffusion modes and an unknown process that give rise to the relatively slowly varying index of refraction fluctuations. We thus refer to this transition as a "homogeneous-to-heterogeneous" (Ho−He) transition.

Evidence that the Ho−He transition is electrical in nature comes from experiments in which a sinusoidal electric field (SEF) was applied across the sample during the DLS experiment.[42,43] Data for the DLS-SEF experiments were collected in the frequency domain, where peaks in the spectral density profile occur at the frequency and harmonics of the applied electric

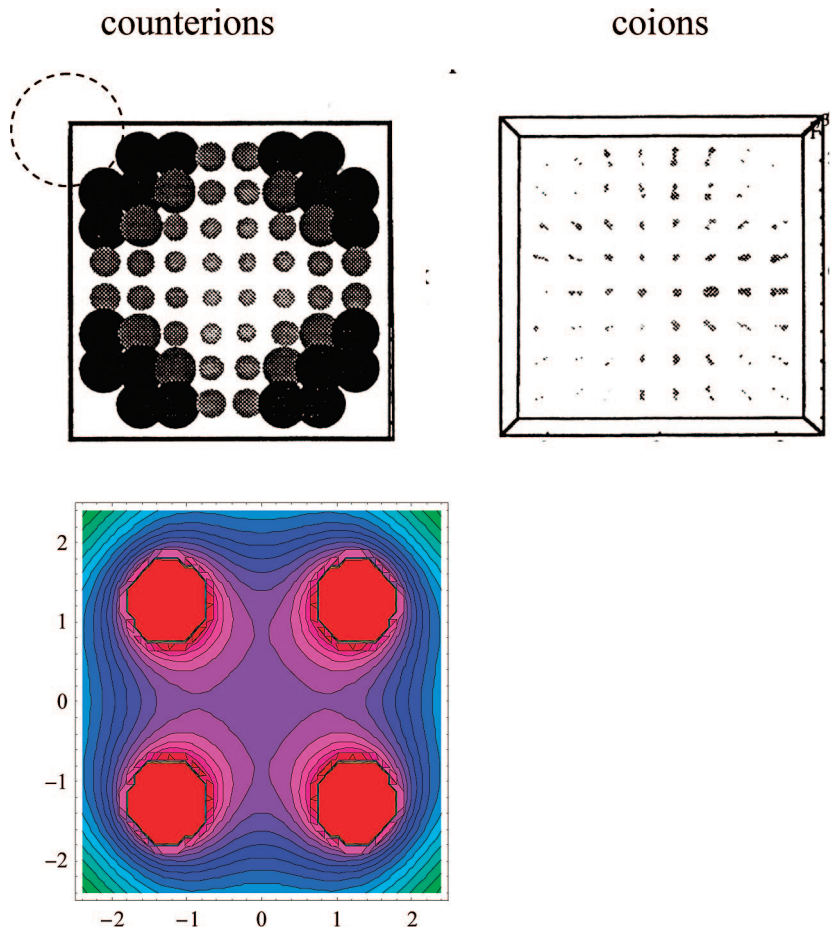

Figure 5. Brownian dynamics and JPF simulations of microion distributions in a cubic array of macroions. The macroion parameters used in the Brownian dynamics and JPF simulations are the same as those used in Figure 2, except that the cell constant is CC = 2.5.

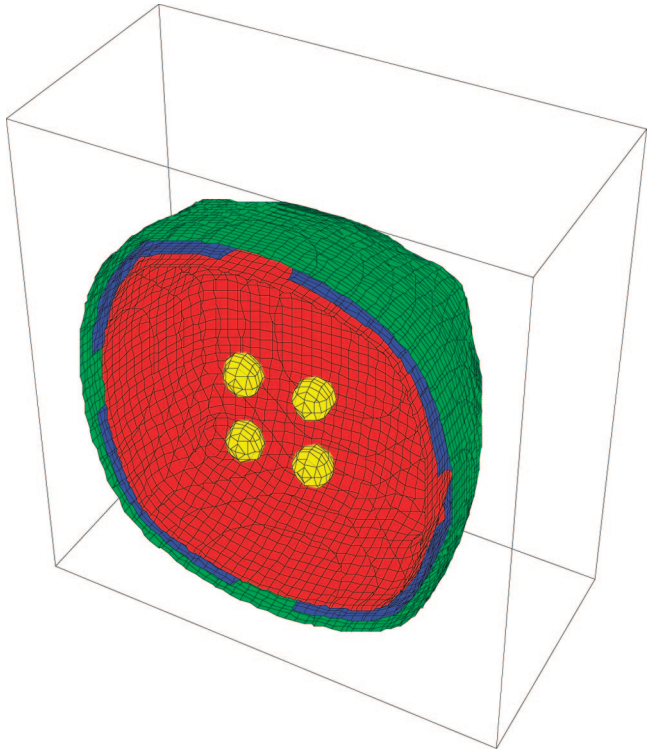

Figure 6. Orbitals of the cubic array of macroions. Shown above are the 3D potential surfaces of the JPF cubic array described in Figure 5. The constant potential values are $\phi_{mac} = 54$ (yellow), $\phi_{mac} = 38$ (red), $\phi_{mac} = 36$ (blue), and $\phi_{mac} = 34$ (green).

field, and a value for D_{app} is obtained from the line width. The sample was $(lys)_{3800}$, and data were obtained for two added salt concentrations: [KCl] = 5×10^{-4} M and [KCl] = 10^{-2} M. The dynamic behavior of the system as determined by DLS experiments verified that 5×10^{-4} M represented the heterogeneous regime and 10^{-2} M represented the homogeneous regime. The driving frequency was 90 Hz. It was reported that the values of D_{app} were virtually identical for both solvents over the range of applied field strengths $3 < E$ (in V/cm) < 30. The "apparent" radius, R_{app}, calculated from D_{app}, decreased in a continuous but nonlinear manner, from $R_{app} = 4000$ Å for $E =$ 3 V/cm to the value $R_{app} = 500$ Å for $E = 30$ V/cm for both solvents. These results indicate that the application of a sinusoidal field at low field strengths can *induce* slow decaying "correlated structures" in the homogeneous regime and at high field strengths can *disrupt* these "correlated structures" in the heterogeneous regime.

A paradox that must be resolved is how the DLS experiments on $(lys)_n$ show a very slow relaxation process that cannot be detected in the FRAP experiments by Zero and Ware.[36] How can macroions behave as if they were independent particles while giving rise to an extraordinarily slow relaxation of index of refraction fluctuations that suggests aggregation of some particles? This "extraordinary" phenomenon has been called *jeu des molecules solmnolentes* (tricks of sleepy molecules) with an apparent diffusion coefficient denoted by D_{jms}.[43,44] Hence, the class II macroions exhibit kinetics heterogeneity but differ from the class I macroions in that they do not form crystalline-like structures in regard to spatial heterogeneity.

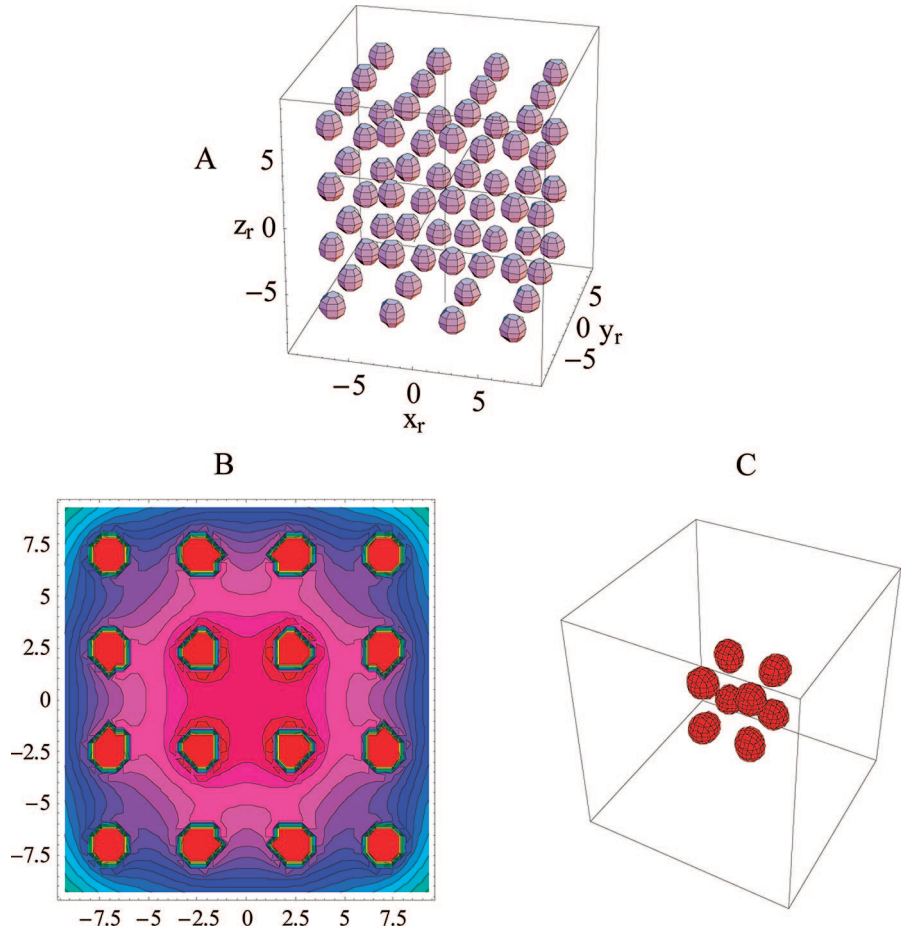

Figure 7. Uniformly distributed macroions in a cubic array. The reference system is a 4 × 4 × 4 cubic array of macroions with a charge $Z_p = 50$ and radius $a_p = 100$ Å. The volume fraction is $\varphi_p = 0.01$, which results in a lattice constant of CC = 4.642, and the length of one side of the box is 18.566, shown in part A. JPF contours in the X_r-Y_r plane at $Z_r = 0$ are shown in part B. Orbitals for the value of $\phi_{mac} = 28.8$, the largest value of ϕ_{mac} that could be displayed, are localized about each of the eight interior macroions, as shown in part C.

A metaphor that might be used as the basis for the interpretation of the paradoxical conclusions drawn from D_T and D_{jms} is a swarm of bees. Viewed from a distance, the movement of a swarm of bees resembles an amorphous density cloud that moves with a group velocity that affects its shape and position. This swarm may hover around a patch of clover, moving from one clover covered area to another. However, upon closer inspection, it is discovered that bees within the swarm change their relative positions within the cluster, and some bees are observed to leave the swarm and other bees enter the swarm. Eventually, the dense swarm of bees dissipates and the collective motions no longer exist. Thus, the time record that describes the movement and dissipation of the swarm is considerably different from that of the motions that describe the individual bees. In a similar manner, the time range that describes the slow dissipation of a cluster of macroions as detected by the index of refraction spatial fluctuation differs from that detected by FRAP experiments for the individual macroions as they enter and leave the region. This is the essence of the "temporal aggregate" model in which a small population of macroions are "temporarily correlated" through the sharing of counterions.[13,14]

To illustrate the concept of a "temporal aggregate", JPF simulations were carried out with 64 macroions of radius $a_p =$ 100 Å with charge $Z_p = 50$. All distances are expressed in units of the macroion radius as defined by eq 3.1. The volume fraction is $\varphi_p = 0.01$, which corresponds to a cubic box with sides of length $L = 18.566$ in reduced coordinates.

What is important in these simulations is not the actual location of the individual particles but the spatial persistence of a constant potential surface as the macroions are randomly moved throughout the box. The size of the macroions was therefore only used to ensure that the particles remain confined to the box. Otherwise, the particles are treated as point particles, leaving open the possibility of overlap of particle volumes. On the basis of the given volume fractions, the probability of any two particles being in the same volume is on the order of $\varphi_p^2 \approx 10^{-4}$.

This exercise addresses the movement of macroions with spatial density larger than that based on a uniform distribution. We chose, therefore, as the reference structure a simple cubic lattice for a uniform distribution of particles for which $\varphi_p =$ 0.01, which has for the lattice constant CC = 4.642. The reference structure is shown in Figure 7A; the JPF profile in the X_r-Y_r plane in Figure 7B; and the orbitals for maximum value of the JPF potential, $\phi_{mac}(max) = 28.8$, in Figure 7C. It is important to note that the value $\phi_{mac}(max) = 28.8$ is the largest value of ϕ_{mac} for this uniform array, and that these orbitals are localized about macroions in the central region of the cluster. Hence, any value of $\phi_{mac} > 28.8$ in the dynamic simulations indicates a cluster of macroions whose separation distances are smaller than the uniform separation distance.

The simulation was carried out by first establishing a value for ϕ_{mac} to use as a criterion for a cluster. Macroions were randomly placed in the simulation box, and the maximum value

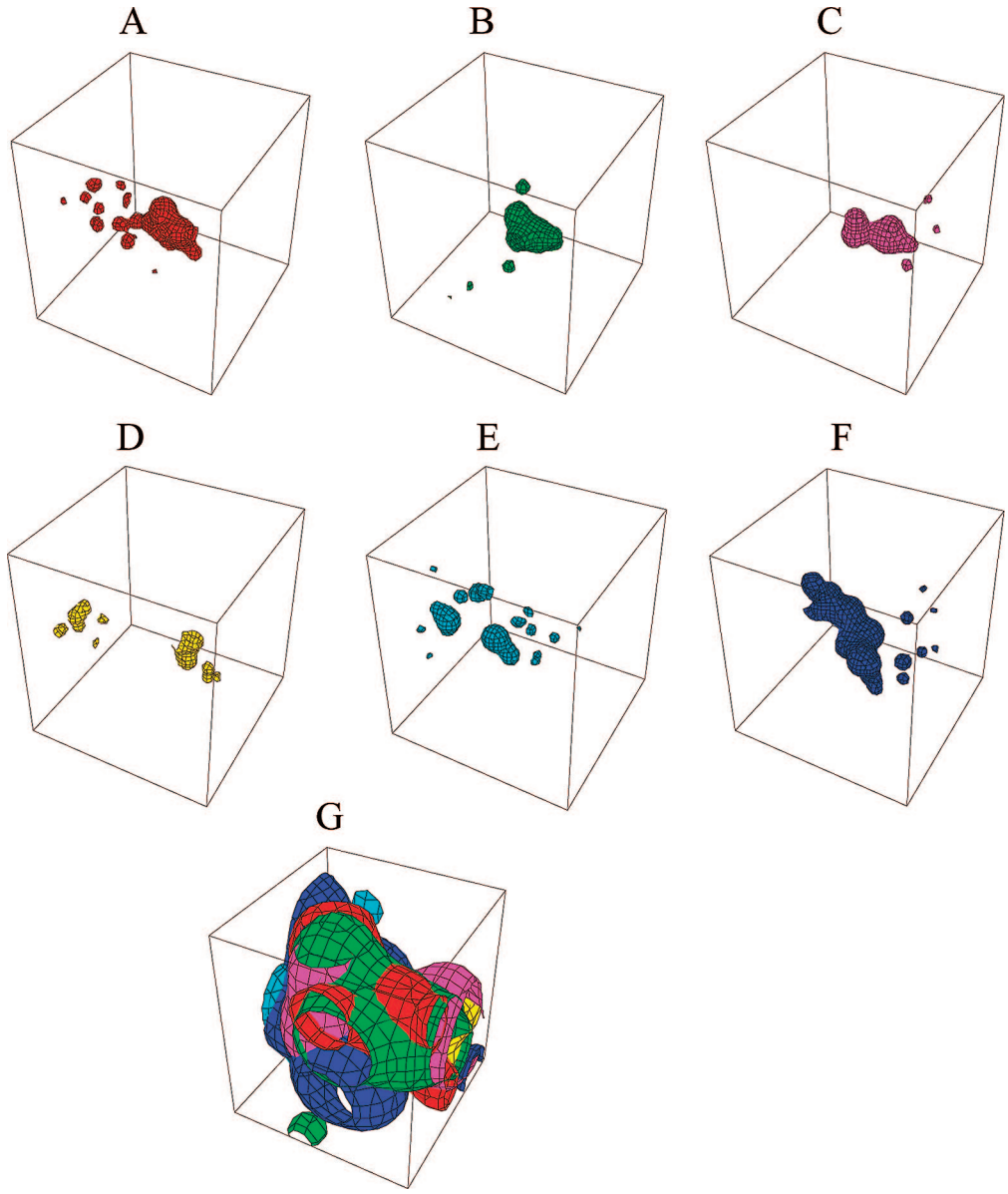

Figure 8. JPF time evolution of concentration fluctuation. An initially random placement of 64 spheres was randomly moved with a random step size in the reduced range $-1 \leq \omega \leq +1$, or a maximum displacement of one macroion radius. The particles were confined to the cubic box corresponding to a volume fraction of $\varphi_p = 0.01$, which corresponds to an external box length of $L = 18.566$ in reduced coordinates. Shown in the above figure are constant potential surfaces for $\phi_{mac} = 36$ after a number of cycles N, where the average root-mean-square (end-to-end) displacement is denoted by rms. The legend for the images is the following: (A) $N = 0$, red; (B) $N = 1$, green; (C) $N = 5$, purple, rms = 1.915; (D) $N = 20$, yellow, rms = 3.793; (E) $N = 40$, turquoise, rms = 5.187; (F) $N = 80$, blue, rms = 6.719. Image G is the superposition of the color coded surfaces in a cubic subregion of relative edge length $\mathbf{l} = 0.3L = 5.57$. The coordinate ranges of the subregion are the following: {{−1.857, 3.713}, {−3.713, 1.857}, {−3.713, 1.857}}.

of ϕ_{mac} was determined for that random distribution. After several trial runs, the value $\phi_{mac} = 36$ was chosen to identify macroion clusters in the subsequent simulations. For the dynamics simulations, the step size S for each coordinate of every particle was randomly generated within the reduced range $-1 \leq S \leq +1$, i.e., the reduced radius of the particle. A search was made for the regions with surface potential $\phi_{mac} = 36$ after the number of cycles N, with color code, where $N = 0$ (red), $N = 1$ (green), $N = 5$ (purple), $N = 20$ (yellow), $N = 40$ (turquoise), and $N = 80$ (blue).

In most of the simulations, potential surfaces were evident for all cycles. In a small number of cases, the clusters "disappeared" for $N > 20$. In one of these latter simulations, the cluster reappeared for $N = 80$. A representative simulation for over 90% of those performed in this study is shown in Figure 8 A−F. As evident in these figures, one might expect appearances of regions for which $\phi_{mac} = 36$ in random regions of the computation cell. Of relevance to the present discourse is the persistence of such surfaces within a particular subregion chosen from the initial configuration. Using the initial configuration shown in Figure 8A, the subregion in the relative coordinate range {{−1.857, 3.713}, {−3.713, 1.857}, {−3.713, 1.857}} was chosen as the target region, which corresponds to a cube of edge length $\mathbf{l} = 0.3L = 5.57$. Shown in Figure 8G is the target region with a superposition of the results in Figure 8A−F. The average end-to-end displacement of all of the particles from their initial positions for $N = 80$ is 6.719. Since this distance is larger than the length of the edge of the target region, all of the particles initially within the target region had a high probability to move outside of the target region. The persistence of the

constant surface potential $\phi_{mac} = 36$ within the target region must be due to the continued replenishment of particles. Eventually, the potential within the target region falls below $\phi_{mac} = 36$ as this fluctuation decays. These simulations illustrate how a system composed of particles that exhibit independent movement, as in the FRAP results, may exhibit a long-lived index of refraction fluctuations, as detected in the DLS studies.

6. Class III - Weakly Charged Macroions and the Formation of "Vesicle-Like" Structures

Our focus is on the hollow, spherical shape $\{Mo_{132}\}$ and the wheel-shape $\{Mo_{154}\}$, and the roles that solvent and macroion charge play on the self-assembly of these macroions. The charge on these macroions is controlled by pH and solvent composition.

The full formula of $\{Mo_{132}\}$ is

$$(NH_4)_{42}[Mo_{72}(VI)\ Mo_{60}(V)O_{372}(CH_3COO)_{30}(H_2O)_{72}] \approx 300H_2O \approx 10CH_3COONH_4$$

where the maximum charge for the fully dissociated macroion is -42.[20] The shape of this macroion is spherical, with a diameter of 2.9 nm.[16] Kistler et al.[15] have performed a series of experiments that characterized the conditions necessary for self-assembly of $\{Mo_{132}\}$ as a function of a water/acetone solvent. The formation of assemblies, detected by static and dynamic light scattering methods, was reported to occur in the range 70% > acetone > 3%. The equivalence of the radius of gyration (R_g) and hydrodynamic radius (R_h) indicated that the assembled structure was a hollow sphere formed by a single layer of macroions. Because $\{Mo_{132}\}$ is itself spherical, the "vesicle-like" assembly was referred to as a "blackberry" structure. The size of the blackberries was dependent upon the solvent composition, ranging from 30 to 100 nm, decreasing in size as the acetone content decreased. The charge of the blackberry structure varied over the range -61 to -200, as estimated from zeta potential measurements depending upon the solvent conditions.[15] These observations mean that the stability of the blackberry structure requires the presence of counterions and depends upon the quality of the solvent. Since the $\{Mo_{132}\}$ macroions are not in contact in the blackberry structure, these authors stated that "...macroions tend to strongly attract one another when they carry enough charges".[15] These studies confirm earlier reports by Liu[16,19] on the $\{Mo_{72}Fe_{30}\}$ macroions, where the surface-to-surface distance for the macroions in the blackberry structure was on the order of 0.9 nm. Above 70% acetone content, the electrostatic interaction between the counterions and the $\{Mo_{132}\}$ is strong, resulting in condensation of the counterions onto the macroion surface leaving a neutral species. At the other extreme, less than 3% acetone, the counterions are completely dissociated from the macroions. Thus, the mutual repulsive interactions between the component macroions make the blackberry structure unstable and only the macroions $\{Mo_{132}\}$ are found in the system.

The complete formula for $\{Mo_{154}\}$ is

$$Na_{15}[Mo_{126}(VI)\ Mo_{28}(V)O_{462}H_{14}(H_2O)_{70}]_{0.5} \times [Mo_{124}(VI)\ Mo_{28}(V)O_{457}H_{14}(H_2O)_{68}]_{0.5} \approx 300H_2O$$

where the release of 15 Na^+ and 14 H^+ results in a charge of -29.[45] The shape of this macroion is like a wheel, or a life preserver found on boats. The outside diameter of the wheel is 3.6 nm.[45] Static and dynamic light scattering studies by Liu and co-workers[17] on the assembly of $\{Mo_{154}\}$ indicate that $R_g \approx R_h$. Hence, the assembly of $\{Mo_{154}\}$ macroions also has a "vesicle-like" structure. These authors also estimated that the center-to-center distance of the $\{Mo_{154}\}$ in the assembly is approximately 4.9 nm. Since this distance is greater than the diameter of $\{Mo_{154}\}$ (3.6 nm), they suggested that water not only fills the gaps but also plays a very important role in "...holding the overall assembly together".[17] This hypothesis is consistent with recent dielectric studies by Oleinikova et al.[45] on $\{Mo_{154}\}$ macroion assemblies. These authors analyzed the spectra of macroion and assembled macroion samples in terms of five modes: bulk water near 20 GHz and four confined modes, near 4 GHz, two in the range 50 MHz to 1 GHz, and an intense mode at 7 MHz. Upon self-association, the peak at 7.2 MHz increased by a factor of 2, that at 90 MHz decreased by more than a factor of 2, and the peak at 800 MHz shifted to 450 MHz (water is more tightly bound). The authors interpret these results as an increase in the water molecules tightly associated between the macroions of the assembled macroions. They concluded that structured water and integrated cations between the wheels result in electrostatic attraction which stabilizes the vesicle structure. This model is in concert with the model previously proposed for the spherical $\{Mo_{72}Fe_{30}\}$ system by Liu and co-workers.[18,20] Schematic representations of the general blackberry structure, the $\{Mo_{132}\}$ macroion subunit, and the proposed counterion-stabilized structure are shown in Figure 9.

JPF simulations were performed with macroions of charge distributions that mimic the spherical $\{Mo_{132}\}$ and wheel-shaped $\{Mo_{154}\}$ macroions in a planar array of relative dimensions of the surface of their respective vesicle superstructures. In the JPF simulation, the $\{Mo_{132}\}$ was represented by a sphere of radius SR = 1.45 nm, which also served as the normalization length. The spherical shape of the macroion was represented by six subspheres of relative radius 0.1 that were symmetrically placed along the axes of an arbitrary coordinate system attached to the macroion. For the purpose of comparison with the JPF profiles for $\{Mo_{154}\}$ of charge -30, the charge of each of the six subspheres was taken to be -5. The cell constant for the planar array of spherical macroions was CC = 3.67 in accordance with the separation distance for the macroions in the blackberry reported by Liu.[16] The macroion $\{Mo_{154}\}$ was represented in the JPF simulation as a disk of radius SD = 1.8 nm, which also served as the normalization length. The charge of the macroion was distributed among 15 subspheres, each of charge -2 and relative radius 0.1, that are uniformly distributed along the rim of the wheel. The cell constant for the planar array of planar macroions was CC = 4.72. The macroion and 4×4 clusters representing $\{Mo_{132}\}$ and $\{Mo_{154}\}$ in Figure 10 and the JPF constant contour mappings are shown in Figure 11. The general features of the contour mappings in Figures 7 and 11 are the same. However, the discrete distribution of charges on the surfaces of the macroions in Figure 11 results in a significant influence on the distribution of particles in the vicinity of the macroion surface. Since the charge on each macroion is -30, the two JPF profiles in Figure 11 also illustrate the effect of charge distribution on the potential field about and within the cluster.

We now propose a specific mechanism for the stability of the blackberry array in the mixed acetone−water solvent. The extent of the dissociation of the counterions from the macroion is dependent upon the polar character of the solvent as proposed by Kistler et al.,[15] that no dissociation occurs in a purely nonpolar solvent and complete dissociation occurs in a purely polar solvent. Hence, partial dissociation of the macroions occurs in the intervening acetone/water mixed solvent, resulting in macroions of relatively low charge.

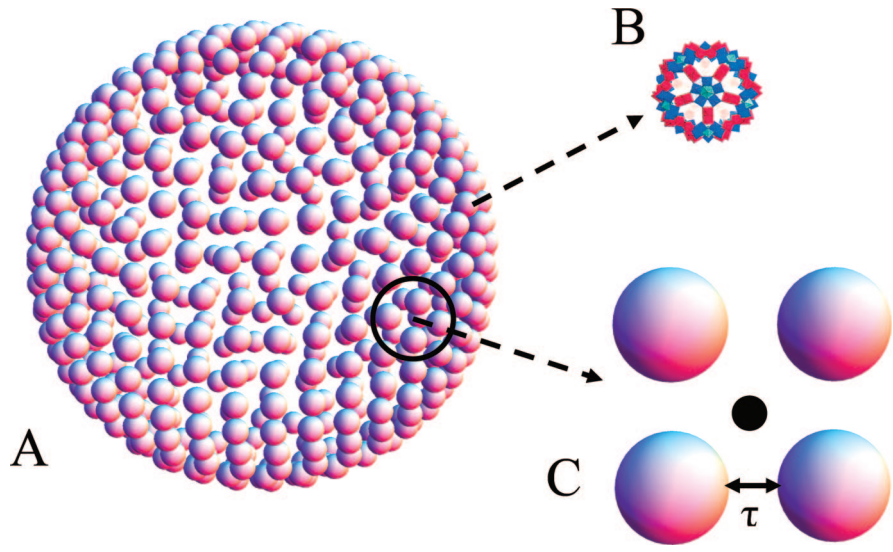

Figure 9. Schematic representation of a blackberry. The blackberry structure is represented in part A, where the spherical subunits are generic representations of the macroions. A cartoon of the $\{Mo_{132}\}$ macroion structure is shown in part B. The mechanism for stabilization of the blackberry structure involves counterions located in the region between the macroions, as proposed by Liu et al.[18,20] and illustrated in part C. The surface-to-surface distance, τ, must be great than zero.

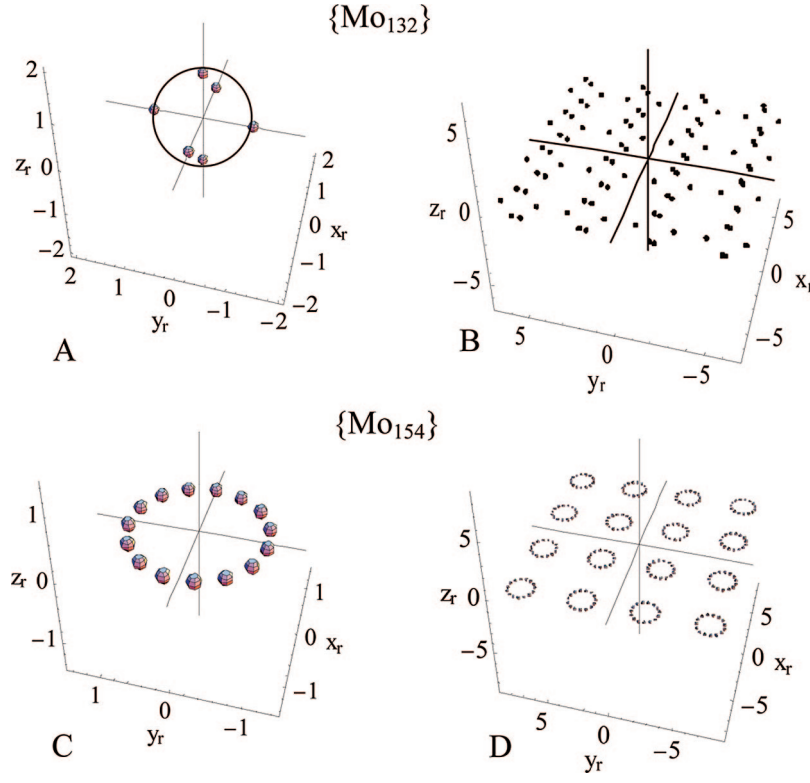

Figure 10. Parameters for simulations of $\{Mo_{132}\}$ and $\{Mo_{154}\}$. The macroion $\{Mo_{132}\}$ is represented as a sphere with radius RS = 1.45 nm and a charge $Z = -30$ which is equally distributed in a spherical arrangement of six subspheres of relative radius 0.1 and charge -5, as shown in part A. These macroions were then placed in a planar array with lattice spacing (in relative units) CC = 3.67, as shown in part B. The macroion $\{Mo_{154}\}$ is represented as a disk with radius RD = 1.8 nm. The charge of the disk was distributed evenly in the rim by 15 spheres of $Z = -2$, with a relative radius 0.1, as shown in part C. These macroions were then placed in a 4×4 planar array with lattice spacing (in relative units) CC = 4.72, as shown in part D.

Water is a polar molecule, and is subject to the electric field in the vicinity of the macroion. Hence, an accumulation of water molecules occurs in the vicinity of the site charges for the mixed solvent. When two macroions of low net charge are brought into close proximity, the water associated with each macroion surface acts to structure the water between the macroions. The range of interaction is inferred from the blackberry structure, where the surface-to-surface distance between the macroions is in the range 0.9−2.4 nm. Assuming the diameter of water to be 0.4 nm, the gap between the macroion surfaces allows at most six water molecules. The local geometry dictated by the curvature of the macroions therefore may be considered to confine these particles, and the external region beyond the influence of the curvature is defined as a reservoir of particles. This geometric description now mimics the model used in computer simulations on

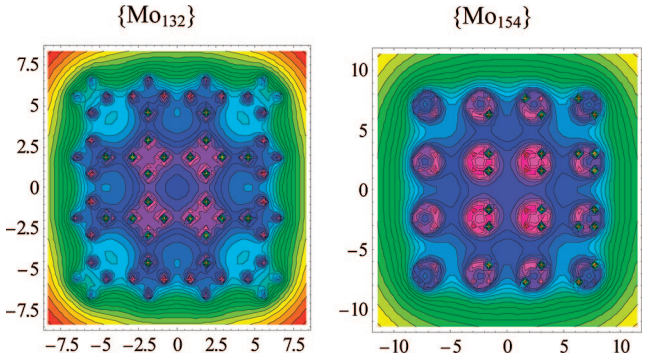

Figure 11. JPF constant contour mappings for clusters of $\{Mo_{132}\}$ and $\{Mo_{154}\}$. JPF profiles in the X_r-Y_r plane at $Z_r = 0$ were obtained for the 4×4 planar arrays of $\{Mo_{132}\}$ and $\{Mo_{154}\}$ as represented by the charge distributions defined in the caption of Figure 10.

confinement of particles between neutral films.[46−48] One may therefore use the results of these simulations to provide additional insight as to the structure of water in this region of the blackberry. In the cited simulations, the surface of the confining films does not interact with the particles. If the particles are themselves neutral, then the results of Boda et al.[46] indicate that there should be no persistent structure of particles in the confined region. If the particles are charged, then the electrostatic repulsion between the particles in solution causes some particles to accumulate at the surface of each film because there is no corresponding repulsion with the film to reject this accumulation.[47,48] Of particular relevance to the curved geometry of macroions is the case of a wedge film, where the gap size ranges from half the particle diameter to 8.5 times the particle diameter.[48] The repulsive interaction between the particles generates a structure in the region between the two surfaces if the gap is large enough to accommodate additional particles. As indicated by the "snapshots" of the wedge in their Figure 4,[8] the structure of the confined charged spheres varies from zero particles, to particles in single file, to particles lining only the surfaces of the wedge, to particles aligned on the wedge surface with a third ordering of particles midway between the surfaces, to apparently random configurations at the broadest region of the wedge. We may infer from these simulations how water molecules might similarly interact with the wedge region between two POM macroions. Rather than purely repulsive interactions, the water molecules interact with each other through their dipole moments. Depending upon their relative orientations, the dipole−dipole interaction may be either attractive or repulsive. To illustrate, we represent the discrete charge on the macroion as [−] and the water dipole as (+ −). In the region of closest approach of the two macroions, one may expect a slight repulsion occurs between the surface-bound water molecules because of their alignment, as well as the repulsive interaction between the charged sites. However, as the gap between the two surfaces increases due to the curvature of the macroions, more water molecules are allowed into the wedge region. These additional water molecules are also aligned in concert with the associated water molecules at the macroion surfaces. Assuming the point of contact at the macroion surface is also a site charge, the extension of the water molecules from the macroion surface into the wedge region is represented by the line:

{[−](+−)(+−)(+−)(+−)},..., {(−+)(−+)(−+)(−+)[−]}

Since these "fingers" radiate from curved surfaces, the extended oriented dipoles generated by the surface-bound water molecules also contribute to the orientation of the other water molecules within the wedge. However, lurking in the solution are the original counterions, represented by the symbol [+], which can form a stabilizing link between "fingers" of the two macroions:

{[−](+−)(+−)(+−)(+−)}[+]{(−+)(−+)(−+)(−+)[−]}

Extension of this mechanism to four macroions in a planar configuration places the stabilizing counterion in the center of dipole oriented water molecules, as illustrated in Figure 9C. The water molecules between the macroions are tightly associated with the macroions and would therefore exhibit a different structure than in the bulk solution. This hypothesis for stabilization is consistent with the previously mentioned dielectric studies by Oleinikova et al.[45] on $\{Mo_{154}\}$. These water−counterion (w−c) bridges thus stabilize the blackberry structure.

Because of the spherical symmetry of the $\{Mo_{132}\}$ and $\{Mo_{72}Fe_{30}\}$ particles, one might expect them to aggregate in a random fashion. The specific question asked by Verhoeff et al.[20] is: "First of all, why do the POMs form single-layer structures?" Verhoeff and co-workers[20] explained the vesicle structure in an *ad hoc* fashion as being a result of surface tension and elastic properties of the vesicle. While this model may explain the stability of single-layered structures, it does not provide a mechanism for the formation of such structures. The proposed w−c mechanism of association of two macroions discussed above may provide some insight to the paradox of how the assembly of spherical objects can lead to structures of well-defined size and geometry.

Consider the situation of four spherical macroions denoted by the letters A, B, C, and D. Let these four macroions be connected through w−c bridges. Envision this assembly of macroions as wandering through configuration space. There are only three conceptual arrangements of the w−c bridges depending upon the relative arrangements of the macroions. If the macroions form a linear structure represented as A−B−C−D, then there are three independent w−c bridges. A second configuration is obtained when three of the macroions form a triangular structure with the fourth exterior to this structure, as represented by (ABC)−D. In this case, there are four w−c bridges: three that connect the (ABC) in a pairwise manner and the fourth connecting the D macroion with the other three. The last conceptual arrangement is when all four macroions are interconnected with shared w−c bridges, such as in a square-planar array. In this case, the number of pairwise w−c bridges between the four macroions is six. If the stability of the cluster of four macroions is increased with the increase of the number of w−c bridges, then the square-planar array is the most stable of those configurations considered. However, what would result if two or more square-planar arrays were to likewise be interconnected through w−c bridges? The answer may lie in the combined effects of direction extension of the bound water and in the resulting surface tension of the structured water in the wedge region between the macroions. For example, two drops of water on a surface will coalesce into one drop when they come into contact. It is therefore more energetically favorable to have all of the w−c bridges coalesce into one continuous structure. As this process continues, the addition of macroions to a previously formed cluster will give rise to a planar structure held together by the network of w−c bridges.

Eventually, the surface of the confined water structure will develop a significant surface tension and elasticity that these effects come into play, resulting in the energy minimization structure of a single layer shell structure. A similar mechanism applies for the wheel structure of $\{Mo_{154}\}$ in forming a vesicle, although the direction of the water bridges may be predetermined to be on the rim and therefore not directed by minimization of energy.

The above mechanism accounts for the very slow kinetics of assembly of the blackberry structure for $\{Mo_{72}Fe_{30}\}$[19] with an activation energy $E_a > 117$ kJ/mol.[49] In addition, orientation constraints implied with the alignment process can also reduce the reaction rate by an order of magnitude or greater.[50]

7. Characteristics of the Transitions in the Charge-Size Landscape

The only characteristic parameters discussed thus far are the *charge-size* coordinates associated with only the heterogeneous landscape of macroion systems. Implicit are the assumptions that the values of the macroion concentrations, added salt concentrations, temperature, solution pH (to change the charge on the macroion), mixed solvent composition, and other parameters are consistent with the stabilization of the heterogeneous system under consideration at the time. Clearly, variation of these additional parameters as well as the *charge-size* coordinates can result in a transition to the homogeneous states, or other heterogeneous states, that comprise the complete landscape accessible to the chosen system. It may be assumed that there are similarities between such transitions within the generalized landscape.

For example, the transition *macroion−vesicle−macroion* diagram in Figure 4 of Kistler et al.[15] as a function of solvent composition resembles the reentrant *liquid−crystalline−liquid* transition that was reported by Yamanaka et al.[51] when the charges of the colloidal silica and polymer latex spheres were changed. An interpretation[52] of the reentrant diagram of Yamanaka et al.[51] was proposed as follows: stage I, the liquid state obtained for weakly interacting particles; stage II, the intermediate charge with extended ion clouds allow for considerable sharing of counterions which stabilizes a crystalline structure; stage III, where the higher charge results in extensive counterion condensation that reduces the coupling of macroions and returns the system to the liquid state. Similarly, Kistler et al.[15] proposed that the solvent composition controls the charge of $\{Mo_{132}\}$ throughout the *macroion−vesicle−macroion* transition. However, the physical processes arising from the change in charge differ greatly for these two systems. As noted by Kistler et al., the charge on the macroion is reduced to virtually the neutral state in the solvent systems for which the acetone concentrations are greater than 70%. Without these stabilizing electrostatic interactions, the blackberry array breaks up. This is the same situation as in stage I for the colloidal silica and polymer latex sphere systems. However, an increase in charge on the $\{Mo_{132}\}$ attained as the acetone content is lowered over the range 70% to pure water does not attain either stage II or stage III characteristics.

To explain the difference in character of the POM systems and the colloidal silica and latex sphere systems upon an increase in charge, one must take not only the magnitude of the charges involved but also take into consideration their sizes relative to the size of the solvent molecules. The POM macroions are less that 4 nm in size compared to the colloidal particles whose size is greater than 100 nm. As can be inferred from the results in section 2, a large macroion more strongly interacts with a test charge than a small macroion even though the surface charge densities are the same. The maximum charge of −42 for $\{Mo_{132}\}$ is not of sufficient magnitude to influence the ion cloud much beyond its vicinity, nor does it have the counterion condensation capacity of the considerably higher charged colloidal silica and polymer latex sphere systems. On the other hand, the smaller size of the POM macroions allows several macroions to form a collection of wedge regions that extend over a significant fraction of their surfaces so as to promote a network of water−counterion bridges. The implication is that there is an upper limit to the size of a macroion than can form stabilizing w−c bridges. Consider the square-planar array of A−B−C−D macroions discussed in section 6, where the macroion radius is a_p and the minimal gap width (surface-to-surface) is τ, as shown in Figure 9. Assume that the distance between the surfaces of two macroions along the diagonal of the square represents the maximum length of a w−c bridge connecting the macroions, and denoted as L_{w-c}. The relationship between L_{w-c}, a_p, and τ is

$$L_{w-c} = \sqrt{2}(2a_p + \tau) - 2a_p \qquad (7.1)$$

Using the $\{Mo_{154}\}$ assembly as an example, with a center-to-center distance of 4.9 nm and the wheel diameter of $2a_p = 3.6$ nm,[45] one obtains from eq 7.1 the value $L_{w-c} = 3.3$ nm for the length of the w−c bridge. This is roughly equivalent to 10 water molecules. Using this value of L_{w-c} as a guide, we can now use eq 7.1 to estimate an upper limit to the size of a macroion that has the potential to form w−c bridges. If we set $\tau = 0$, then the operational relationship becomes $L_{w-c} \approx 0.83a_p$. If we allow for the possibility that a w−c bridge can contain 20 water molecules, then the upper limit of the radius of a macroion to form stable assemblies by w−c bridges is $a_p(\max) = 6.6/0.83 = 7.9$ nm. What this means, physically, is that for a collection of macroions with a radius larger than 7.9 nm the interstitial solvent is best described in terms of the reservoir properties than that of the wedge region in accordance with the model of Trokhymchuk et al.[48]

8. Discussion

The physical nature of a system of charged particles must be viewed from the vantage point of the entire system. This is clearly illustrated in the studies of Tohver et al.[53] on a system of highly charged nanoparticles (3 nm in size) and essentially neutral silica microspheres (285 nm in size). This mixed system exhibited a *gel−fluid−gel* transition as the relative concentration of the nanoparticles increased. Note that in this system the central state is the *fluid* state, whereas in the systems discussed in the previous section the central state was the *heterogeneous* state. The reason for this "interchange" has to do with the mechanisms involved. For low concentrations of nanoparticles, the virtually neutral microparticles undergo flocculation because of the short-range van der Waals attractive forces. What is of interest in the current discussion is the mechanism proposed for the stability of the fluid state. As is well-known, a purely repulsive interaction will lead to a uniform distribution of charged particles throughout the system, where the presence of the walls of the container prevents further separation of the charged particles. In the nanoparticle/microsphere system, the microspheres offer "neutral regions" scattered throughout the system. The cumulative effect of the repulsive interactions between all of the charged nanoparticles in the system is to

"force" these charged particles toward the surface of the neutral sphere, since it offers no repulsive force to keep them away. As a result, the concentration of the charged nanoparticles is higher in the vicinity of the neutral microsphere than in the bulk medium. That is, the total repulsive interaction of the nanoparticles in the bulk medium is considerably greater than the repulsion of the local nanoparticles in the vicinity of the microsphere. If one were to look *only* in the vicinity of a single microsphere, one might conclude that there is an *attractive interaction* between the microspheres and the single nanoparticle. However, this conclusion would be incorrect because the *apparent attractive interaction* is actually due to the *cumulative repulsive interactions* of the charged nanoparticles throughout the solution. Langmuir likewise took the holistic approach in his model for coacervates based on the uniformity of the chemical potential throughout the medium.[21] This holistic approach is now applied to the systems discussed in this study.

Attention is first given to the system of large macroions that can attain a charge large enough to condense counterions. To simplify the discussion, all parameters are held constant except the charge of the macroion and the corresponding change in the counterion concentration. As the charge of the macroion builds up, the range of its influence extends further into the supporting medium at a rate faster than the released counterions can add additional screening effects. Eventually, the spheres of influence of the macroions begin to overlap. What this means to maintain a constant chemical potential in the region between the macroions is that the counterion concentration must likewise increase. Eventually, a situation is obtained where the counterions are influenced by several macroions, and this multiple servitude of the counterions results in a correlation in the dynamics of the participating macroions. An appropriate metaphor for the spheres of influence of a macroion is a box of inflated balloons. An increase in the charge of the macroion to extend its *sphere of influence* is envisioned to be equivalent to blowing up all of the balloons in the box. Eventually, every balloon in the box will be touching all of its neighbors, and the balloons will be uniformly distributed throughout the box. If we now attempt to continue to blow up all of the balloons, there will be a huge stress put on the system, where some of the balloons might even burst. One way to alleviate this stress is to collapse some of the balloons so that others may expand. In the macroion system, the electrical stress is alleviated by the condensation of counterions by some of the macroions. This gives rise to a "two-state" system in a manner similar to the micelle clusters examined by Langmuir,[21] where the charge on the clustered micelles is less than those in the bulk medium so that the chemical potential remains constant throughout the system. Note the similarity in the holistic mechanism of this system with that of Tohver et al.[53] The electrical stress put on the charged nanoparticles and highly charged macroions results in a "condensation" of the smaller charged particles onto the surface of the larger particles, but with opposite outcomes. The condensation of nanoparticles onto the microspheres disrupts the cluster in favor of stabilizing the fluid state, whereas the condensation of counterions onto the macroion particles results in pockets of macroion clusters throughout the medium.

However, not all macroions can achieve a charge high enough to influence the ion clouds about other macroions. This "charge limitation" is a physical limitation based on the total number of groups on the molecule that can be charged. Hence, not all macroions can achieve class I and class II status. Similarly, not all macroions can achieve class III status. As indicated in section 7, the key to the w−c mechanism is the size of the macroions relative to the size of the polar solvent molecules. A necessary condition is that a significant fraction of the surface area of the macroions be identified with the wedge region when in the assembled configuration. An upper limit to the radius of the macroion for class III status is 8 nm.

Although none of the macroion systems examined herein encompass all three *charge-size* classes of heterogeneous systems, the proposed mechanisms do make predictions regarding the characteristics of a macroion system that can span the entire range. The macroion must have a radius less than 8 nm and be able to attain a net charge in excess of 1000.

References and Notes

(1) Verwey, E. J.; Overbeek, J. T. G. *Theory of the Stability of Lyophobic Colloids*; Elsevier Publishing Co., Inc.: New York, 1948.
(2) Ise, N.; Okubo, T.; Ito, K.; Dosho, S.; Sogami, I. *Langmuir* **1985**, *1*, 176.
(3) Dosho, S.; Ise, N.; Ito, K.; Iwai, S.; Kitano, H.; Matsuoka, H.; Nakamura, H.; Okumura, H.; Ono, T.; DSogami, I. S.; Ueno, Y.; Yoshida, H.; Yoshiyama, T. *Langmuir* **1993**, *9*, 394.
(4) Ito, K.; Yoshida, H.; Ise, N. *Science* **1994**, *263*, 66.
(5) Yoshida, H.; Ise, N.; Hashimoto, T. *J. Chem. Phys.* **1995**, *103*, 10146.
(6) Yoshida, H.; Yamanaka, J.; Koga, T.; Koga, T.; Ise, N.; Hashimoto, T. *Langmuir* **1999**, *15*, 2684.
(7) Lee, W. I.; Schurr, J. M. *Chem. Phys. Lett.* **1976**, *38*, 71.
(8) Lee, W. I.; Schurr, J. M. *J. Polym. Sci., Polym. Phys. Ed.* **1975**, *13*, 873.
(9) Lin, S.-C.; Lee, W. I.; Schurr, J. M. *Biopolymers* **1978**, *17*, 1041.
(10) Drifford, M.; Dalbiez, J.-P. *Biopolymers* **1985**, *24*, 1501.
(11) Drifford, M.; Dalbiez, J.-P. *J. Phys., Lett.* **1985**, *46*, L311.
(12) Schmitz, K. S.; Ramsay, D. J. *J. Colloid Interface Sci.* **1984**, *105*, 388.
(13) Schmitz, K. S.; Lu, M.; Singh, N.; Ramsay, D. J. *Biopolymers* **1984**, *23*, 1637.
(14) Ramsay, D. J.; Schmitz, K. S. *Macromolecules* **1985**, *18*, 2422.
(15) Kistler, M. L.; Bhatt, A.; Liu, G.; Casa, D.; Liu, T. *J. Am. Chem. Soc.* **2007**, *129*, 6453.
(16) Liu, T. *J. Am. Chem. Soc.* **2002**, *124*, 10942.
(17) Liu, T.; Diemann, E.; Li, H.; Dress, A. W.; Müller, A. *Nature* **2003**, *426*, 59.
(18) Liu, T.; Imber, B.; Diemann, E.; Liu, G.; Cokleski, K.; Li, H.; Chen, Z.; Müller, A. *J. Am. Chem. Soc.* **2006**, *128*, 15914.
(19) Liu, T. *J. Am. Chem. Soc.* **2003**, *125*, 312.
(20) Verhoeff, A.; LKistler, M. L.; Bhatt, A.; Pigga, J.; Groenewold, J.; Klokkenburg, M.; Veen, S.; Roy, S.; Liu, T.; Kegel, W. K. *Phys. Rev. Lett.* **2007**, *99*, 066104.
(21) Langmuir, I. *J. Chem. Phys.* **1938**, *6*, 873.
(22) Schmitz, K. S. *Langmuir* **1999**, *15*, 4093.
(23) Bader, R. F. W.; Slee, T. S.; Cremer, D.; Kraka, E. *J. Am. Chem. Soc.* **1983**, *105*, 5061.
(24) Bader, R. F. W. *Acc. Chem. Res.* **1985**, *18*, 9.
(25) Sánchez-Sánchez, J. E.; Lozada-Cassou, M. *Chem. Phys. Lett.* **1992**, *190*, 202.
(26) Schmitz, K. S. In *Handbook of Polyelectrolytes and Their Applications*; Tripathy, S. K., Kumar, J., Nalwa, H. S., Eds.; American Scientific Publ.: Stevenson Ranch, CA, 2002; Vol. 3, pp 195−269.
(27) Schmitz, K. S. *Phys. Rev. E* **2002**, *66*, 0614031.
(28) Messina, R.; Holm, C.; Kremer, K. *Europhys. Lett.* **2000**, *51*, 461.
(29) Messina, R.; Holm, C.; Kremer, K. *Phys. Rev. Lett.* **2000**, *85*, 872.
(30) Messina, R.; Holm, C.; Kremer, K. *Eur. Phys. J. E* **2001**, *4*, 363.
(31) Messina, R.; Holm, C.; Kremer, K. *Phys. Rev. E* **2001**, *64*, 021405.
(32) Messina, R. *Physica A* **2002**, *308*, 59.
(33) Mukherjee, A. K.; Schmitz, K. S.; Bhuiyan, L. B. *Langmuir* **2003**, *19*, 9600.
(34) Mukherjee, A. K.; Schmitz, K. S.; Bhuiyan, L. B. *Langmuir* **2004**, *20*, 11802.
(35) Rouzina, I.; Bloomfield, V. A. *J. Phys. Chem.* **1996**, *100*, 9977.
(36) Zero, K.; Ware, B. R. *J. Chem. Phys.* **1984**, *80*, 1610.
(37) Martin, N. B.; Tripp, J. B.; Shibata, J. H.; Schurr, J. M. *Biopolymers* **1979**, *18*, 2127.
(38) Shibata, J. H.; Schurr, J. M. *Biopolymers* **1979**, *18*, 1831.
(39) Wilcoxon, J. P.; Schurr, J. M. *J. Chem. Phys.* **1983**, *78*, 3354.

(40) Bruno, K. R.; Mattice, W. L. *Macromolecules* **1992**, *25*, 327.
(41) Bruno, K. R.; Mattice, W. L. *Polym. Commun.* **1989**, *30*, 310.
(42) Schmitz, K. S.; Ramsay, D. J. *Biopolymers* **1985**, *24*, 1247.
(43) Schmitz, K. S.; Ramsay, D. J. *Macromolecules* **1985**, *18*, 933.
(44) Schmitz, K. S.; Ramsay, D. J. *J. Colloid Interface Sci.* **1985**, *105*, 388.
(45) Oleinikova, A.; Weigärtner, H.; Chaplin, M.; Diemann, E.; Bögge, H.; Müller, A. *ChemPhysChem* **2007**, *8*, 646.
(46) Boda, D.; Chan, K.-Y.; Henderson, D.; Wasan, D. T.; Nikolov, A. D. *Langmuir* **1999**, *15*, 4311.
(47) Trokhymchuk, A.; Henderson, D.; Nikolov, A.; Wasan, D. T. *J. Phys. Chem. B* **2003**, *107*, 3927.
(48) Trokhymchuk, A.; Henderson, D.; Nikolov, A.; Wasan, D. T. *Langmuir* **2005**, *21*, 10240.
(49) Liu, G.; Liu, T. *Langmuir* **2005**, *21*, 2713.
(50) Schmitz, K. S.; Schurr, J. M. *J. Phys. Chem.* **1972**, *76*, 534.
(51) Yamanaka, J.; Yoshida, H.; Koga, T.; Ise, N.; Hashimoto, T. *Phys. Rev. Lett.* **1998**, *80*, 5806.
(52) Schmitz, K. S. *Langmuir* **2001**, *17*, 8028.
(53) Tohver, V.; Smay, J. E.; Bream, A.; Braun, P. V.; Lewis, J. A. *Proc. Natl. Acad. Sci. U.S.A.* **2001**, *98*, 8950.

JP805648A